RSC Advances

Cite this: *RSC Advances*, 2012, **2**, 9011–9021

www.rsc.org/advances

PAPER

Electrochromic device response controlled by an *in situ* polymerized ionic liquid based gel electrolyte†

Rambabu Sydam,[a] Melepurath Deepa*[a] and A. K. Srivastava[b]

Received 28th February 2012, Accepted 26th July 2012
DOI: 10.1039/c2ra20360j

Polymer electrolytes were synthesized by two different approaches and applied to electrochromic devices based on electrodeposited tungsten oxide (WO_3) or poly(3,4-ethylenedioxythiophene) (PEDOT) films as the cathode, and a Prussian blue (PB) film as the anode. The first method involved the entrapping of an ionic liquid in a polymer host (poly(methylmethacrylate) or PMMA) and the second approach relied on the *in situ* thermal polymerization of methylmethacrylate (MMA) in the hydrophobic ionic liquid, yielding a solidified transparent gel. The effect of *in situ* solid polymer electrolyte formation on device performance characteristics was realized in terms of a larger coloration efficiency of 119 $cm^2\ C^{-1}$ (λ = 550 nm) achieved for the WO_3–PB (MMA) device, as compared to a value of 54 $cm^2\ C^{-1}$ obtained for the WO_3–PB (PMMA) device. Similar enhancements in electrochromic coloring efficiency, reflectance contrast, and faster switching kinetics were obtained for the PEDOT–PB (MMA) device. The strategy of introducing an electrolyte to the electrochromic device in a liquid state and then subjecting the same to gradual polymerization allows greater accessibility of the electrolyte ions to the active sites on the electrochromic electrodes and superior interfacial contact. As a consequence, larger optical contrast and faster kinetics are achieved in the MMA based devices. While PEDOT films were amorphous, PB films were semi-crystalline but only in the case of WO_3; the hexagonal structure of WO_3, equipped with three/four/six-coordinated voids was found to affect bleaching kinetics favorably. The performance of PMMA based electrolyte is limited by high resistance at the electrode–electrolyte interface, and a smaller number of ions available for oxidation and reduction. Large area (~10 cm × 4 cm) devices were also fabricated using this simple wet chemistry method and their ability to color uniformly without any pinholes was demonstrated.

1. Introduction

Electrochromic windows, by dynamically controlling the amount of light and solar energy that can pass through the device, help save energy in buildings and automobiles.[1–3] They consist of two complementary coloring electrochromic layers that change optical properties persistently and reversibly when an electrical voltage is applied. These devices require a very low dc voltage (~1.0–3.0 V) and only use energy to change their optical state, not to maintain any particular state. Typically, response times vary from a few seconds to a few minutes, depending upon the size of the device. The technology can thus save substantial amounts of energy in buildings and automobiles. Among various solar control windows that are commercially available today, such as suspended particle devices, photochromic, thermochromic, tinted and reflective glass, electrochromic windows are the ones that offer the best compromise between electric lighting and cooling energy.[3–5]

The challenge in electrochromic devices is therefore to develop low cost processes and components to enable the fabrication of devices capable of delivering high contrast ratios and long term durability. Tungsten oxide and poly(3,4-ethylenedioxythiophene), or PEDOT, find widespread applications as cathodically coloring electrodes in electrochromic smart windows, dynamic displays, eyewear and variable reflectance devices like mirrors.[6–9] The ability of tungsten oxide to sustain tens of thousands of repetitive cycles of coloration and bleaching, high optical transparency in the visible and infrared regions, in the fully oxidized state, and good UV and chemical stability, render it an efficient electrode in electrochromic devices.[3,4] Similarly, PEDOT films offer stable color switching between light transmissive blue and deep blue colors, are cost effective, have a moderately low band gap in the range 1.5 to 1.6 eV and possess large electronic conductivity in the doped form, thus enabling their use as electrochromic electrodes in smart windows.[10,11] Prussian blue (PB) is an ideal choice for the counter electrode, as it undergoes a complementary color switch between Prussian white ($[Fe^{II}Fe^{II}(CN)_6]^{2-}$, Everitt's salt), which appears as a thin

[a]*Department of Chemistry, Indian Institute of Technology Hyderabad, Yeddumailaram 502205, Andhra Pradesh, India*
[b]*National Physical Laboratory, Dr K.S. Krishnan Road, New Delhi 110012, India*
† Electronic supplementary information (ESI) available: See DOI: 10.1039/c2ra20360j

transparent film and is formed upon electrochemical reduction of Prussian blue ($[Fe^{III}Fe^{II}(CN)_6]^-$, PB).[12] The electrolyte or the ion conducting medium is also an important component of the device, and the use of solid polymer electrolytes aids in the formation of leakage free laminated devices. In the past, a few reports have either focused largely on the properties of polymer electrolytes or evaluated the electrochromic response of electrochromic devices or films,[13–20] but a combination of electrolyte properties and how it affects the darkening/bleaching phenomena in electrochromic devices is relatively less investigated.

Among various studies on electrochromic devices, one report on display devices of small dimensions based on thin walled nanotubes of PEDOT is particularly noteworthy, as the devices showed very fast switching times of about 10 ms.[21] Another study of significance focused on the formation of PEDOT–poly(aniline) devices wherein the electrodes were fabricated using a layer-by-layer assembly and bleaching times of the order of sub-seconds were attained, but the dimensions of the device were not large.[22] In a recent study, PEDOT–PB devices of 12 × 15 cm^2 dimensions, containing an ionic liquid based gel electrolyte, were fabricated using flexible substrates.[23] Yet another report that must be mentioned emphasised devices wherein polyester-based foils were used as substrates; one was coated with a tungsten oxide film colored by sputtering in the presence of H_2 and another with a nickel–vanadium oxide film colored by post-deposition ozone exposure.[3] These films were laminated together by a poly(methyl methacrylate) or PMMA-based electrolyte and the devices were able to endure 5000 color–bleach cycles, without undergoing any significant loss in color contrast.[3] In the past, we have also investigated electrochromism and electrochemistry of PEDOT based cells containing poly(vinyl alcohol) based on free standing electrolyte films of about 5 × 5 cm^2.[24,25]

Despite sustained efforts in the area of fabrication and characterization of electrochromic devices, a systematic study on how the procedure used for electrolyte application to a device influences the electrochromic behavior of the ensuing devices remains unreported to date. Keeping these aspects in view, in the present report, we fabricated electrochromic devices based on PEDOT–PB and WO_3–PB and used two different approaches for synthesizing a polymer electrolyte based on a hydrophobic ionic liquid, and applying the same to these devices. The first method involved the direct application of a gel polymeric electrolyte to a cavity created by a spacer on the electrochromic electrode and sealing. In the second approach, the electrolyte containing the monomer is injected into a pre-sealed electrochromic device in the liquid state and subjected to *in situ* thermal polymerization, to bring about the solidification of the electrolyte solution. Comparison of the electrochromic performance characteristics of the PEDOT–PB and WO_3–PB devices based on the *in situ* polymerized gel electrolyte *versus* a conventional polymeric electrolyte showed dramatic differences in terms of absorbance/reflectance modulation, coloration efficiency, redox response, color–bleach kinetics and charge transport characteristics. Despite the complexity of the comparison, owing to the multiple components of the device, our study attempts to provide an understanding of how the electrolyte incorporation method can alter the electrochromic response of the devices.

2. Experimental

2.1. Materials

Tungsten (W) metal powder (<100 μm), potassium ferricyanide ($K_3[Fe(CN)_6]$), ferric chloride ($FeCl_3$), polyethylene glycol 400 (PEG), 1-butyl-1-methyl pyrrolidinium bis(trifluoromethylsulfonyl)imide, benzoyl peroxide (with 25% H_2O) and reagents: acetone, HCl, methanol, isopropanol, hydrogen peroxide (H_2O_2, 30%) of GR/AR grade were obtained from Merck and used as received. Methylmethacrylate (MMA), camphorsulfonic acid (CSA), 3,4-ethylenedioxythiophene (EDOT) and poly(methylmethacrylate) (PMMA, M.W. = 996 000) were procured from Sigma Aldrich. Ultrapure water (resistivity ~18.2 MΩ cm) obtained through the Millipore Direct-Q 3 UV system was used as the solvent.

2.2. Synthesis of electrochromic films

Tungsten (W) metal powder (13.0 g) was dissolved in 80 mL H_2O_2 at ~50–60 °C and decomposition of the excess peroxide was accomplished by refluxing at the same temperature for 2–3 h. To the resulting turbid solution, 8 mL PEG and 30 mL isopropanol were added, which was followed by filtration to yield a clear yellow precursor solution. Potentiostatic electrodeposition was performed in a three electrode electrochemical cell with a platinum sheet as the auxiliary electrode, a SnO_2:F coated glass substrate as the working electrode, and the reference electrode was Ag–AgCl–KCl. A constant potential of −1.2 V was applied for five minutes, and a blue colored film formed on the working electrode. The SnO_2:F coated glass substrates procured from Pilkington were 4 mm thick, and had a sheet resistance of 14 Ω sq^{-1}. The films were transparent; these were rinsed in deionized water and dried in air. Dissolution of 0.1 M EDOT, 0.1 M $LiCF_3SO_3$, 1.2 M camphorsulfonic acid (CSA) in 15 mL deionized water and 10 mL isopropanol resulted in a colorless solution. The solution was magnetically stirred for thirty minutes at room temperature. The clear solution was used for the oxidative electropolymerization of EDOT onto transparent conducting SnO_2:F coated glass substrates under potentiostatic conditions (+1.2 V), in a three electrode system with another SnO_2:F coated glass substrate as counter electrode and Ag–AgCl–KCl as the reference electrode, for three minutes. The films were rinsed in methanol and stored in air. Prussian blue films were grown from a solution of 10 mM $K_3[Fe(CN)_6]$ and 10 mM $FeCl_3$ in 0.01 M HCl in a three electrode electrochemical cell using Ag–AgCl–KCl as the reference electrode by applying a fixed potential of ~1.5 V for 300 s to a SnO_2:F coated glass substrate. The films were washed in a solution of 0.01 M HCl and deionized water mixed in a 2 : 3 volume ratio and stored in air.

2.3. Synthesis of electrolytes and devices

In the first approach, an acrylic adhesive tape (640 μm thick and 3 mm wide) was applied along the four edges of the glass on the cathodically coloring electrode (WO_3 or PEDOT) and the complementary electrode (PB) was then placed above this electrode and two 1 to 2 mm wide openings were grafted in the tape along one edge. Except for the two openings, the remainder of this assembly was sealed with an epoxy. MMA was passed

through an activated neutral alumina column, to remove the inhibitor. To the ionic liquid, 1-butyl-1-methyl pyrrolidinium bis(trifluoromethylsulfonyl)imide, 30 wt% MMA was added and benzoyl peroxide (1 wt% relative to MMA) was used as an initiator. The electrolyte was injected using a glass syringe through one of the open ports in the device, and the device was then placed vertically in an oven for *in situ* thermal polymerization at 60–70 °C for 24–36 h. Upon polymerization of the liquid in the device, the open ports were sealed with an epoxy. In the second approach, poly(methylmethacrylate) was dissolved in the ionic liquid 1-butyl-1-methyl pyrrolidinium bis(trifluoromethylsulfonyl)imide (15–25 wt%), by continuous stirring at 50–60 °C for eight to ten hours until a clear homogeneous transparent gel was obtained. An open faced cavity was fabricated on the PEDOT or WO_3 electrode using an adhesive acrylic tape and it was filled with the gel electrolyte and heated in the oven at 60 °C, until a bubble free electrolyte was obtained. The counter electrode (PB) was then fixed onto this electrode and the whole configuration was held in place with binder clips. The device was sealed along the entire periphery of the device using epoxy and cured at room temperature. The devices based on *in situ* polymerized gel have been designated as WO_3–PB (MMA) and PEDOT–PB (MMA) and the devices prepared by direct application of the polymeric gel electrolyte were named as WO_3–PB (PMMA) and PEDOT–PB (PMMA) devices.

2.4. Characterization techniques

The optical density of devices for coloration efficiency calculations was measured *in situ*, on a Shimadzu UV-Visible-NIR 3600 spectrophotometer under dc potentials of different magnitudes (applied for a 90 s duration). Specular reflectance measurements under different dc potentials in the visible region (applied for 90 s each) were carried out in a standard mirror/device assembly using a MR 19-1 specular reflection accessory on a T90+ UV-Vis spectrophotometer. All measurements were performed with respect to a control device, devoid of any electrochromic coating, but containing the polymer (PMMA or MMA based) electrolyte, and the conducting glass substrates. The electrochemical charges intercalated/deintercalated during redox switching of the devices were determined by chronoamperometry. Cyclic voltammetry (CV) was performed for the devices with PEDOT or WO_3 as the working electrode and PB as the auxiliary electrode, in a two-electrode configuration (the reference was shorted with the counter electrode during the measurement) (Fig. S1, ESI†). The electrochemical potential stability window (measured by CV) and optical transmittance *versus* wavelength for the polymer electrolytes are shown in Fig. S2 (ESI†). All electrochemical measurements and electropolymerization were performed on an Autolab PGSTAT 302N coupled with NOVA 1.6 software. The electrochromic switching response of the devices was performed under square wave potentials, at a fixed monochromatic wavelength, at a constant frequency, using a Shimadzu UV-Visible-NIR 3600 spectrophotometer, in kinetic mode. Switching of the films was also measured on Avantes (Avaspec-2048) coupled with Autolab, in spectroelectrochemical mode in a quartz cell; the instrument was capable of scanning wavelengths from 400 to 800 nm in 1 ms. Electrochemical impedance spectroscopy was performed on the devices in the frequency range 0.05 Hz to 10^6 Hz by superposition of an ac voltage of 10 mV over a zero dc potential. A thin layer of film (WO_3 or PEDOT or PB) was carefully extracted using forceps in deionized water and then transferred onto a carbon coated copper grid, 3.05 mm in diameter, and the solvent was evaporated at room temperature. A high resolution transmission electron microscope (HRTEM) FEI Tecnai G2 F 30 STWIN with a FEG source operating at 300 kV was used for structural analysis. The surface roughness of the films was measured using a Nanosurf Easy Scan atomic force microscope. X-Ray diffraction (XRD) patterns were recorded on an XRD, PANalytical, X'PertPRO instrument with Cu-Kα (λ = 1.5406 Å) radiation. For all device characterization, device dimensions of ~3 cm × 3 cm were employed, unless mentioned otherwise, owing to constraints posed by the sample compartment dimensions for different studies.

3. Results and discussion

3.1. Fabrication of electrochromic devices

In an electrochromic device, an ion conducting electrolyte separates the two electrochromic layers, and together the layers and the electrolyte allow the transport of electrons and ions. We preferred a pyrrolidinium ion based ionic liquid as the electrolyte, as, due to its non-aromatic character (in comparison to an imidazolium ion), the pyrrolidinium electrolyte is known to be electrochemically more stable than the imidazolium electrolyte and is therefore more suitable for electrochromic or electrochemical devices.[26,27] In the device, one layer acts as the positive electrode (*e.g.* Prussian blue) and another layer (*e.g.* tungsten oxide) serves as the negative electrode. When a voltage is applied, cations stored in the positive electrode traverse to the negative electrode, a phenomenon that converts transparent tungsten oxide to a tungsten metal bronze (a light-absorbing blue layer) formed by the electrochemical intercalation of ions. Concurrently, the anodic Prussian blue layer undergoes oxidation and attains a deep blue color, which is complementary to the color change experienced by the cathodic tungsten oxide film. The longer the period for which the bias is applied, the more ions are inserted and the darker the device becomes.[4,5] On reversing the applied voltage, the process is also reversed.

A schematic illustrating the differences in fabrication of MMA and PMMA based devices is shown in Fig. 1a and b. For fabricating the MMA based devices, the injection filling technique was used. Two open ports of about 2 mm each were created on the spacer strip affixed to a Prussian blue film (Fig. 1c) and the red adhesive tape was removed, as shown in the figure. The PEDOT or the WO_3 coated glass substrate, with the electroactive layer facing inwards, was placed on the acrylic tape and allowed to cure. The MMA electrolyte in the liquid state was then injected through one of the open ports using a syringe, and then the whole device assembly was heated for *in situ* thermal polymerization. Upon solidification of the electrolyte, the two ports were sealed with an epoxy and ready for use. For synthesizing PMMA based devices, the spacer was applied along all four edges of the Prussian blue film without leaving any gaps (Fig. 1d). The PMMA based gel electrolyte was carefully filled into the cavity with a glass rod, and the assembly was heated until a bubble free electrolyte layer was obtained (Fig. 1d). At

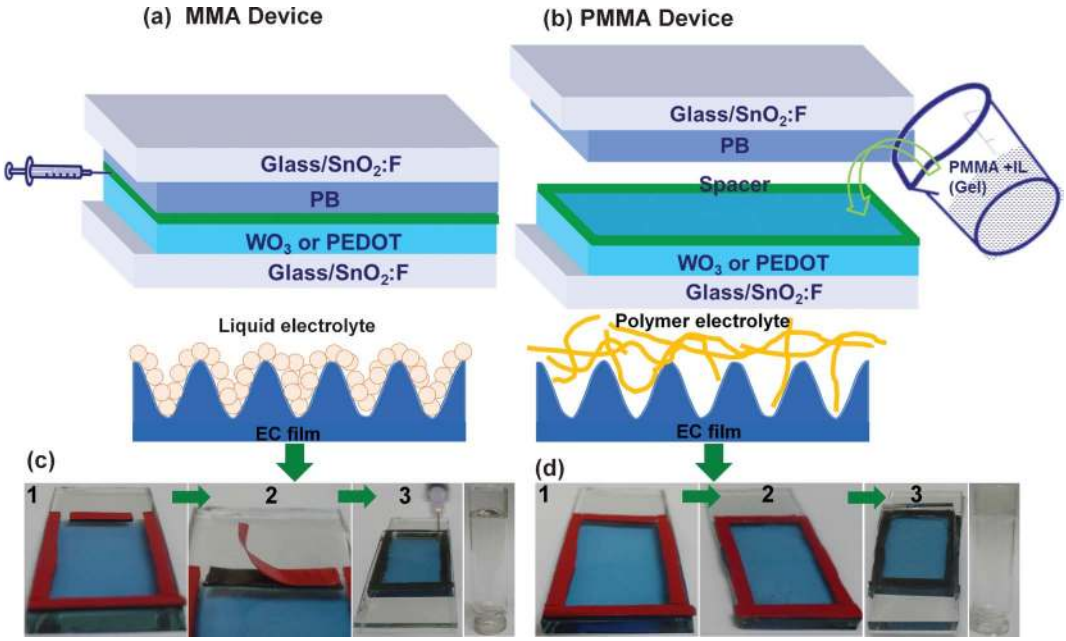

Fig. 1 Schematics of the protocols used for device fabrication in (a) MMA and (b) PMMA based devices and the corresponding electrode–electrolyte interface in each case. The sequence of steps followed in the fabrication of (c) MMA based devices: (1) open ports on a PB layer with a spacer, (2) removal of adhesive tapes and (3) application of a WO_3 layer and injection of electrolyte and (d) PMMA based devices: (1) creation of cavity with a spacer on a PB layer, (2) cavity filled with PMMA electrolyte and (3) removal of red adhesive tape and application of WO_3 layer. The inverted vials in (c) and (d) are photographs of MMA and PMMA electrolytes.

this juncture, the red overlying tape was removed and the complementary electrochromic film (PEDOT or WO_3) was placed on this assembly. Upon curing at room temperature, the devices were sealed with epoxy prior to use. Both MMA and PMMA based gels have hardly any flow properties at room temperature, as can be seen from their photographs shown in Fig. 1c and d. The gels do not flow even when the vials are turned upside-down.

3.2. Spectroelectrochemistry of WO_3–PB devices

The *in situ* absorbance spectra of WO_3–PB (MMA) and WO_3–PB (PMMA) devices measured under different oxidation potentials (applied to WO_3) of +0.5 to +1.5 V and reduction potentials of −0.5 to −3.5 V (in steps of 0.5 V) are shown in Fig. 2a and b, respectively. All ΔOD_{max} for the devices were determined from the difference between fully colored and bleached states and these are summarized in Table 1. As can be seen from Table 1, the WO_3–PB (MMA) device shows a much larger absorbance change (ΔOD_{max}) in contrast to the WO_3–PB (PMMA) device, at all wavelengths extending even to the NIR region, up to 1700 nm. For instance, a $\Delta OD_{1060(max)} = 1.75$ was achieved for the WO_3–PB (MMA) device in comparison to a $\Delta OD_{1060(max)}$ of 0.62 obtained for the WO_3–PB (PMMA) device. Coloration efficiencies of the devices at monochromatic wavelengths of 550, 633 and 1060 nm were deduced from the appropriate linear fits from the ΔOD *versus* charge density plots, which are shown in Fig. 2c and d and are also listed in Table 1.

Coloration efficiency (CE or η), which is defined as the optical density change (ΔOD) induced as a function of the injected electronic charge per unit area to produce the optical change is given by

$$\eta\ (\lambda) = \Delta OD\ (\lambda)/(Q/A) \quad (1)$$

or by

$$\eta\ (\lambda) = \log\ (T_b(\lambda))/\log\ (T_c(\lambda))/(Q/A) \quad (2)$$

where η ($cm^2\ C^{-1}$) is the coloration efficiency at a given wavelength, T_b and T_c are the transmission in the bleached and colored states at a given wavelength.[4] The coloration efficiency for the WO_3–PB (MMA) based device was 119 $cm^2\ C^{-1}$ at a photopic wavelength of 550 nm (the wavelength at which the human eye is most responsive) as compared to a value of only 54 $cm^2\ C^{-1}$ at the same wavelength for the WO_3–PB (PMMA) based device. The MMA based device continued to show much higher coloration efficiencies at other wavelengths as well (Table 1). On examining the data of a poly(aniline)–polyhedral oligomeric silesquioxane–WO_3 device, we found that it showed a CE of 84 $cm^2\ C^{-1}$ (λ_{max} = 625 nm) and a ΔOD of ∼0.7 under a potential switch of ±2 V.[9] In another recent report, for a WO_3 film deposited on a PET (poly(ethylene terepthalate)) electrode of carbon nanotubes, a ΔOD of 1.7 and a coloration efficiency of 64 $cm^2\ C^{-1}$ were achieved in a liquid electrolyte of $LiClO_4$ in PC.[28] Our values are superior to the reported values of ΔOD and CE.

Photographs of WO_3–PB (MMA) devices of ∼4 cm × 10 cm dimensions are shown in bleached and colored states in Fig. 2e and f. The high uniformity of the colored state across the device is apparent, indicating that the device is most suitable for electrochromic window applications. The MMA based device shows larger CE values than the PMMA based one, as in the former device the electrolyte is injected in the liquid state and can therefore easily percolate through the pores of the WO_3 film, and subsequent to the solidification of the electrolyte by *in situ* thermal polymerization two possibilities exist. An intimate contact is established between the WO_3 electrode and polymer electrolyte,

Table 1 Electrochromic parameters for WO_3–PB devices, where ΔOD_{max} = OD (−3.5 V) − OD (+1.5 V) and CE = $\Delta OD_{max}/Q$(−3.5 V)/area

Device	λ (nm)	ΔOD_{max} (a.u.) MMA	ΔOD_{max} (a.u.) PMMA	CE (cm^2 C^{-1}) MMA	CE (cm^2 C^{-1}) PMMA
WO_3–PB	550	0.79	0.20	119	54
WO_3–PB	633	1.00	0.29	149	80
WO_3–PB	1060	1.75	0.62	203	147

which facilitates ion transfer at the electrode–electrolyte interface and, secondly, a greater number of electrolyte ions can access the film, thus leading to a higher contrast and an enhanced coloration efficiency (as shown in the schematic of Fig. 1a). Once the electrolyte is adsorbed, upon application of the reduction potential, the three, four and six coordinated voids provided by the hexagonal structure of WO_3[4,29] can easily entrap the cations from the electrolyte. We ascertained the presence of hexagonal channels in WO_3 films by high resolution transmission electron microscopy (HRTEM), which is discussed in the following section.

3.3. HRTEM of electrochromic films

The TEM image of WO_3 film shows a pine-tree like morphology and these long shapes with tapered ends are interconnected and uniformly distributed across the film (Fig. 3a). Such a pine-tree like structure has been observed for $W_{18}O_{49}$ by heating WS_2 in oxygen.[30] The high magnification image shown in the inset of Fig. 3a shows these elongated fiber like shapes to be composed of WO_3 grains of no particular shape, typical of WO_3 films deposited by surfactant mediated electrodeposition.[31] The HRTEM image of the same film shown in Fig. 3b reveals lattice fringes of WO_3 with inter-planar spacings of 0.32 and 0.39 nm, which matches well with the hexagonal crystalline structure of WO_3, as per JCPDS card number 33-1387. The d-lines correspond to the (200) and (001) reflections of hexagonal WO_3. The inverse fast Fourier transform (IFFT) imaging process was performed to filter out the noise in the real space HRTEM image and the enhanced lattice image was reproduced and is

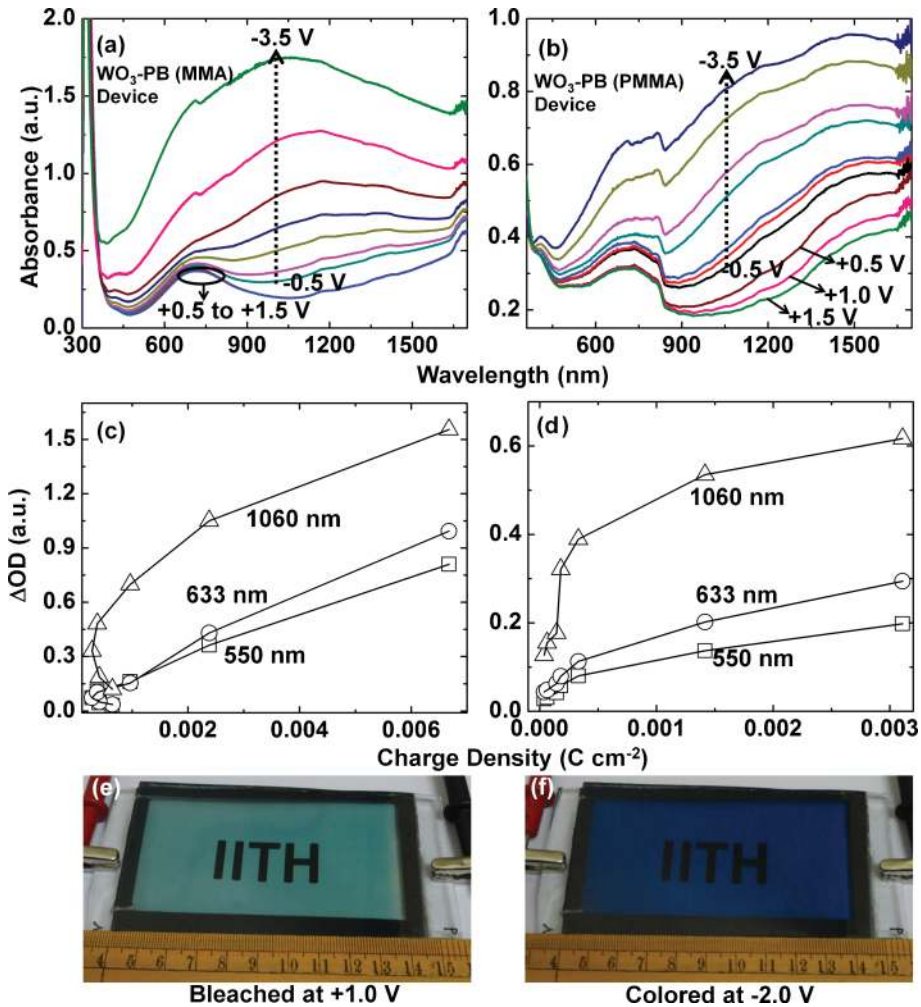

Fig. 2 *In situ* absorbance spectra of (a) WO_3–PB (MMA) and (b) WO_3–PB (PMMA) devices in the wavelength range 350–1700 nm recorded under oxidation potentials of +0.5, +1.0 and +1.5 V and under reduction potentials of −0.5 V to −3.5 V, in steps of 0.5 V, applied for 90 s each. Optical density change *versus* charge density plots of (c) WO_3–PB (MMA) and (d) WO_3–PB (PMMA) devices; photographs of the WO_3–PB (MMA) device in (e) bleached and (f) colored states.

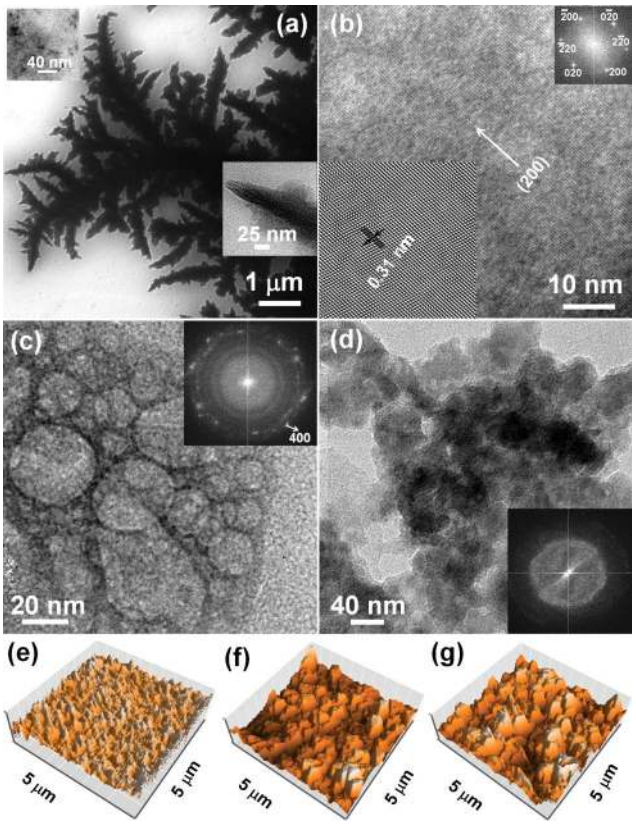

Fig. 3 (a) Bright field image of a WO_3 film; insets on left and right are high and low magnification images, respectively, (b) HRTEM image of WO_3, inset on right is an IFFT of the same, TEM images of a (c) PB and (d) a PEDOT film; insets of (b), (c) and (d) show the corresponding electron diffraction images generated by FFT. Three dimensional AFM images of (e) WO_3, (f) PB and (g) PEDOT films.

shown as an inset of Fig. 3b. The lattice fringes in this inset are extremely sharp and an atomic scale resolution could be achieved. The fringe spacing is 0.31 nm and corresponds to the (200) plane of hexagonal WO_3 in accordance with the JCPDS card number 33-1387. There are hardly any dislocations or defects indicating the high crystalline quality of WO_3 grains. This was also confirmed from the XRD pattern which showed a preferred orientation for hexagonal WO_3 along the (200) plane (Fig. S3, ESI†). Fast Fourier transformation (FFT) was also performed and the resulting electron diffraction pattern is shown as an inset of Fig. 3b. Bright spots conforming to a hexagonal crystal structure of WO_3 are observed, which agrees well with the lattice scale image. Hexagonal WO_3 has octahedral and tetrahedral voids, which can act as channels for ion-insertion and extraction during coloration and bleaching.[4,29] The bright field image of the PB film shown in Fig. 3c reveals the presence of well-connected large aggregates, and the electron diffraction pattern generated by FFT (inset of Fig. 3c) shows the presence of bright spots superimposed on diffuse rings. PB has a face centered cubic crystalline structure and the white spots originate from this crystal phase. The TEM image of PEDOT film (Fig. 3d) shows aggregates of polymer particles and the diffraction pattern produced by FFT shows broad and diffuse rings characteristic of the amorphous nature of the polymer.[32] The three dimensional AFM images of the three films are shown in Fig. 3(e–g). The WO_3 nodules are more compactly packed as compared to PEDOT or PB and the WO_3 films have a relatively smoother texture in comparison to PEDOT or PB. This is also reflected in the significantly lower root mean square surface roughness of 1.3 nm as compared to values of 24.6 nm and 28.3 nm obtained for PB and PEDOT films respectively. A moderately high value of surface roughness enhances the electrolyte adsorption capacity of the film, which can result in higher contrast ratios.

3.4. Spectral response of PEDOT–PB devices

The absorbance variation and coloration efficiency plots as a function of wavelength and applied potential for PEDOT–PB (MMA) and PEDOT–PB (PMMA) devices are shown in Fig. 4 and 5. Unlike the WO_3–PB (MMA) device, the PEDOT–PB (MMA) device remains slightly blue even in the bleached state (Fig. 4b), due to the highly absorptive nature of oxidized PEDOT in the visible region. A maximum absorbance change of 1.27 was registered for the MMA based device at a λ_{max} of 600 nm (Fig. 4a). The broad absorption in the NIR region in the oxidized form of PEDOT is due to the bipolaronic transitions, which lose intensity at the expense of the π–π^* transition peak (at 600 nm), with increasing reduction potential. Photographs of the PEDOT–PB (MMA) device of $\sim$3 cm $\times$ 5 cm dimensions in the dark blue and pale blue states are shown in Fig. 4b. PEDOT based devices could not be up-scaled to the dimensions of WO_3 based ones, as on increasing the area of deposition, a high degree of non-uniformity was observed.

A similar trend for OD variation was observed for the PEDOT–PB (PMMA) device. A ΔOD_{max} of 1.79 (with +1.5 V as the reference potential) was achieved at a λ_{max} of 610 nm (Fig. 5). In a similar manner to the WO_3–PB devices, the PEDOT–PB devices also retained a large optical change in the NIR region. Coloration efficiency plots for the PEDOT–PB (MMA) device as a function of wavelength and at different reduction potentials are shown in Fig. 4c and d and the values are listed in Table 2. The reference potential was chosen as +1.5 V for the calculations. A coloration efficiency maximum of 287 $cm^2\ C^{-1}$ was registered for this device at a λ_{max} of 567 nm, under a fairly low reduction potential of -0.7 V, which is most advantageous for maximizing the operation lifetime of the device. In the past, for a poly(propylenedioxythiophene)–$(Et)_2$–PB device, an unusually high coloring efficiency of 1214 $cm^2\ C^{-1}$ was obtained.[33] In another study on a PEDOT–In_2O_3:Sn–PET film, a coloration efficiency of 124 $cm^2\ C^{-1}$ and a ΔOD of $\sim$0.26 was observed at 540 nm.[28] However, in both these reports, the values were achieved in a liquid electrolyte: $LiClO_4$–PC (propylene carbonate). In another report, for a PEDOT–gel–PB device, prepared using PET substrates, with a gel containing $Li(CF_3SO_2)_2N$, 1-butyl-3-methyl imidazolium imide and PMMA, a CE of 335 $cm^2\ C^{-1}$ was attained and a ΔOD of $\sim$0.77 was observed.[23] The CE plot for the PEDOT–PB (PMMA) device in Fig. 5b shows this device to have a CE_{max} of 267 $cm^2\ C^{-1}$ at $\sim$695 nm (under $E = -1.5$ V). CE values were lower at other potentials. It is obvious that the PMMA based device requires a higher potential ($E = -1.5$ V) to acquire a CE_{max}, whereas an external bias of only -0.7 V, was sufficient for reaching a higher value of CE_{max} in its MMA counterpart. A smaller amount of charge

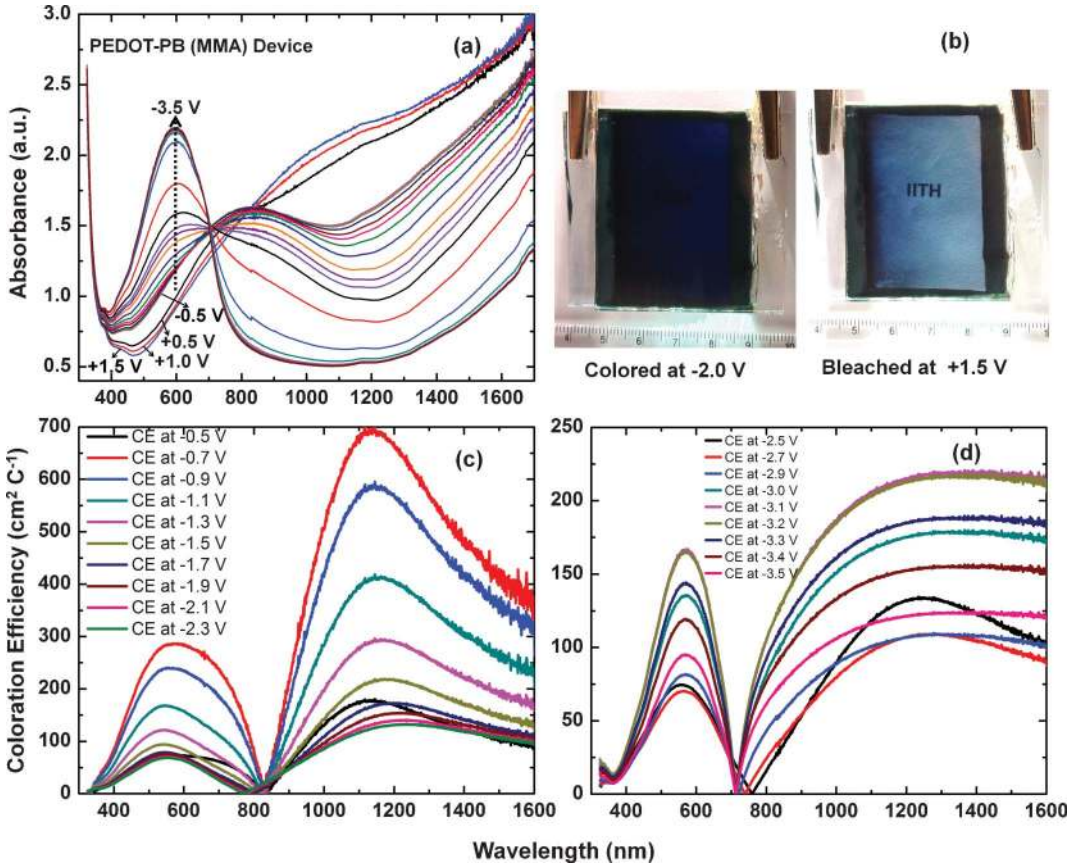

Fig. 4 (a) *In situ* absorbance spectra of a (a) PEDOT–PB (MMA) device in the wavelength range 350–1700 nm recorded under oxidation potentials of +0.5, +1.0 and +1.5 V and under reduction potentials of −0.5 V to −2.9 V, in steps of 0.2 V and from −3.0 to −3.5 V, in steps of 0.1 V, applied for 90 s each. (b) Photographs of a PEDOT–PB (MMA) device in the colored and bleached states, coloration efficiency plots of the PEDOT–PB (MMA) device as a function of wavelength for reduction potentials between (c) −0.5 and −2.3 V and (d) −2.5 and −3.5 V; the optical state under +1.5 V in (a) was chosen as a reference.

suffices to generate a greater electrochromic efficiency in the MMA based device, which is beneficial for prolonging the functional lifetime of the device. We must mention that the CE plots for the PMMA based devices for $E > 1.5$ V are not shown here, and the wavelength range was limited to a maximum of 1000 nm, in comparison to a limit of 1600 nm for the MMA based device, as the curves for the PMMA were noisy, possibly due to increased scattering of radiation by the electrolyte under high potentials.

The specular reflectance variation as a function of wavelength in the visible region of the devices was measured under oxidation and reduction potentials within the range +2.5 V to −3.5 V (Fig. 6). The PEDOT–PB (PMMA) device showed extremely small changes in reflectance with potential, (Fig. S4, ESI†), due to low transparency even in the oxidized state. Permanent pyrrolidinium ion entrapment in the electrodes, which results in irreversible coloration, could be responsible for the poor reflectance modulation (ΔR). The ΔR_{max} values are listed in Table S1 (ESI†). Again, the WO_3–PB (MMA) and the PEDOT–PB (MMA) devices showed higher values of ΔR_{max} as compared to their PMMA counterparts (Table S1, ESI†). Although the magnitude of reflectance modulation is lower than the corresponding absorptive modulation of these devices, nevertheless ΔR values are reasonably high for their application in reflective electrochromic devices. The superiority of electrolyte filling by injection and *in situ* thermal polymerization is obvious. Our values are comparable to values reported in the literature for devices of smaller dimensions. Earlier, for a PEDOT based device, a reflectance contrast of 40% was achieved at a photopic wavelength of 573 nm for 95% of the full switch.[6]

3.5. Switching kinetics

Coloration-bleaching characteristics of PEDOT–PB (MMA) and WO_3–PB(MMA) devices recorded at monochromatic wavelengths (λ_{max}) of 585 and 685 nm, with 3 and 5 s as step times, under a square wave potential of ± 2.0 V, are shown in Fig. 7. The time required for absorbance to increase from 10% to 90% of its full switch in a half cycle is the coloration time, and the time required for absorbance to decrease from 90% to 10% of its total magnitude is the bleaching time. Under a step time of 3 s (Fig. 7a) a coloration time of 2.0 s and a bleaching time of 2.2 s was observed for the PEDOT–PB (MMA) device. For the WO_3–PB(MMA) device (Fig. 7b), color time was 2.1 s and bleach time was 1.7 s (half cycle time is 3 s). Coloration kinetics is faster than bleaching for the PEDOT based device, whereas bleaching is faster than coloration for the WO_3 based device. Since, in the bleaching cycle, the back EMF opposes the applied potential, the diffusion of the cations from the WO_3 film is hindered as the

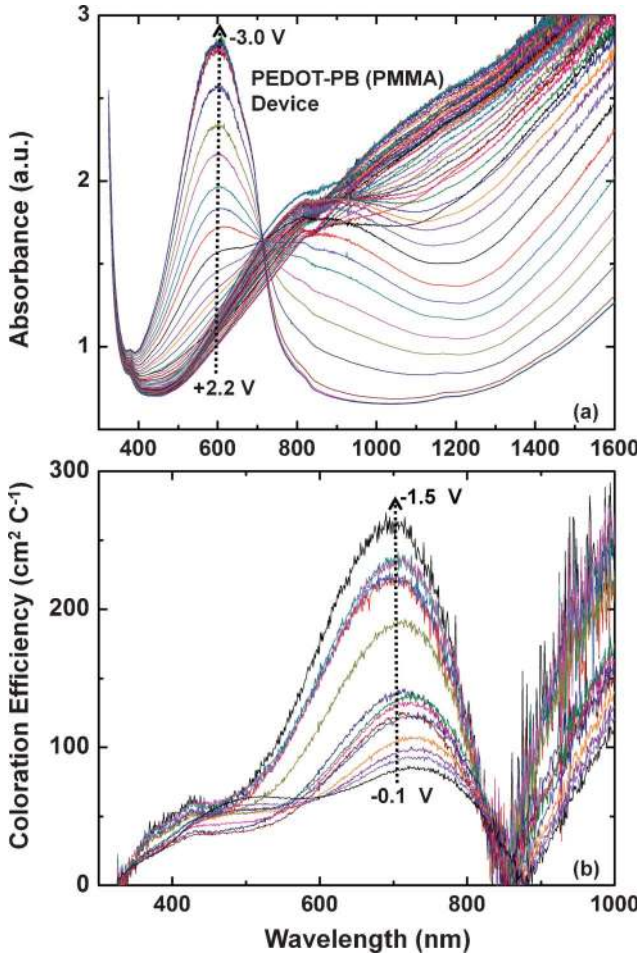

Fig. 5 (a) *In situ* absorbance spectra of a (a) PEDOT–PB (PMMA) device recorded under potentials of +2.2 V to −3.0 V, in steps of 0.1 V, applied for 90 s each and (b) coloration efficiency of a PEDOT–PB (PMMA) device as a function of wavelength for reduction potentials between −0.1 and −1.5 V; the optical state under +1.5 V in (a) was chosen as a reference.

pyrrolidinium ion is a bulky organic molecule and as a result bleaching takes longer. Also, in oxides the film morphology is known to affect bleaching more than coloration, and therefore the hexagonal structure of WO_3 allows faster deintercalation. In the PEDOT based devices, it is the anion insertion and extraction from the polymer film that controls switching rates. Coloration is faster here, as imide ion extraction is facilitated by

Table 2 Electrochromic parameters for PEDOT–PB devices, where ΔOD = OD (−0.7 V) − OD (+1.5 V) (for MMA based) and ΔOD = OD (−1.5 V) − OD (+1.5 V) (for PMMA based) and CE = ΔOD/Q(−0.7 V or −1.5 V)/area

E for CE_{max} (V) MMA	λ (nm)	CE_{max} (cm^2 C^{-1}) MMA	E for CE_{max} (V) PMMA	λ (nm)	CE_{max} (cm^2 C^{-1}) PMMA
−0.7 V	567 $(\lambda_{max})_{vis}$	287	−1.5 V	695 $(\lambda_{max})_{vis}$	267
−0.7 V	550	283	−1.5 V	550	108
−0.7 V	633	274	−1.5 V	633	217
−0.7 V	1145 $(\lambda_{max})_{NIR}$	706	−1.5 V	993 $(\lambda_{max})_{NIR}$	282

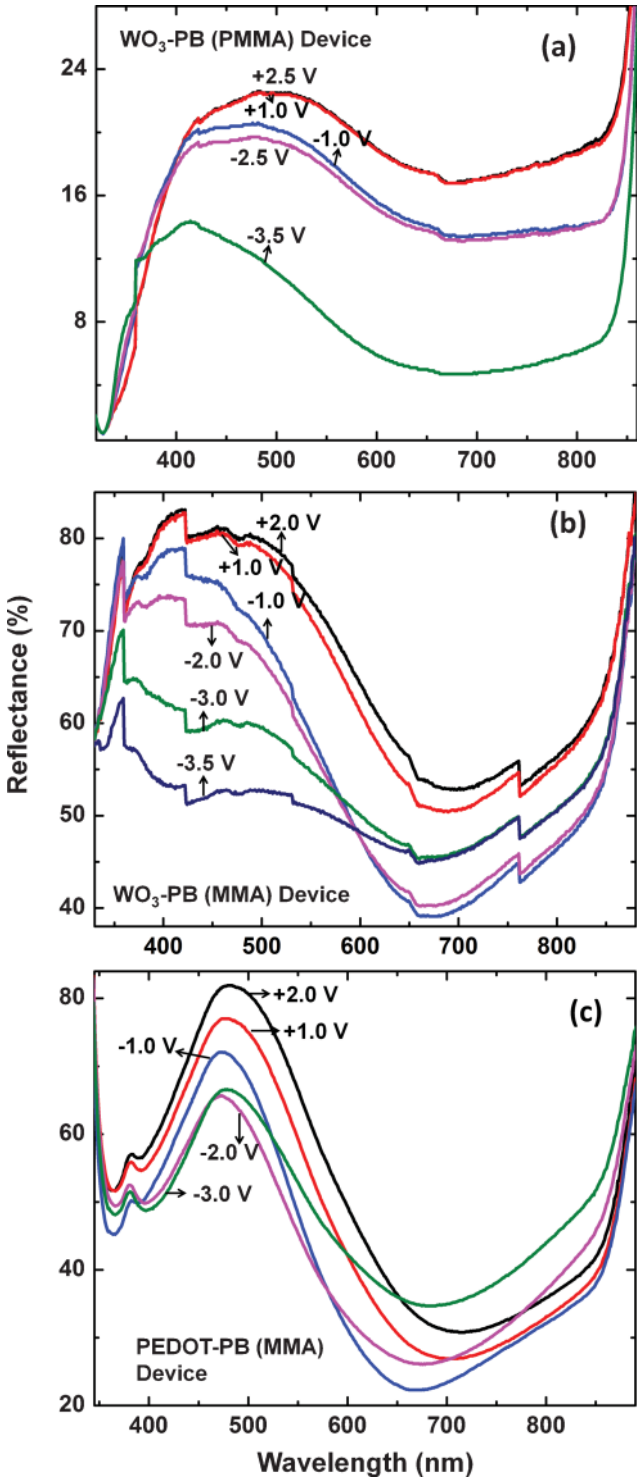

Fig. 6 *In situ* specular reflectance of (a) WO_3–PB(PMMA), (b) WO_3–PB(MMA) and (c) PEDOT–PB (MMA) devices *versus* wavelength, recorded with respect to a standard mirror/control device assembly under different dc potentials in the range +2.5 V to −3.5 V.

the large separation between polymer chains caused by the expansion of the molecular network upon incorporation of camphorsulfonate counterions used during oxidative electropolymerization of EDOT. Coloration of PEDOT is also accompanied by the transition from the conducting doped state

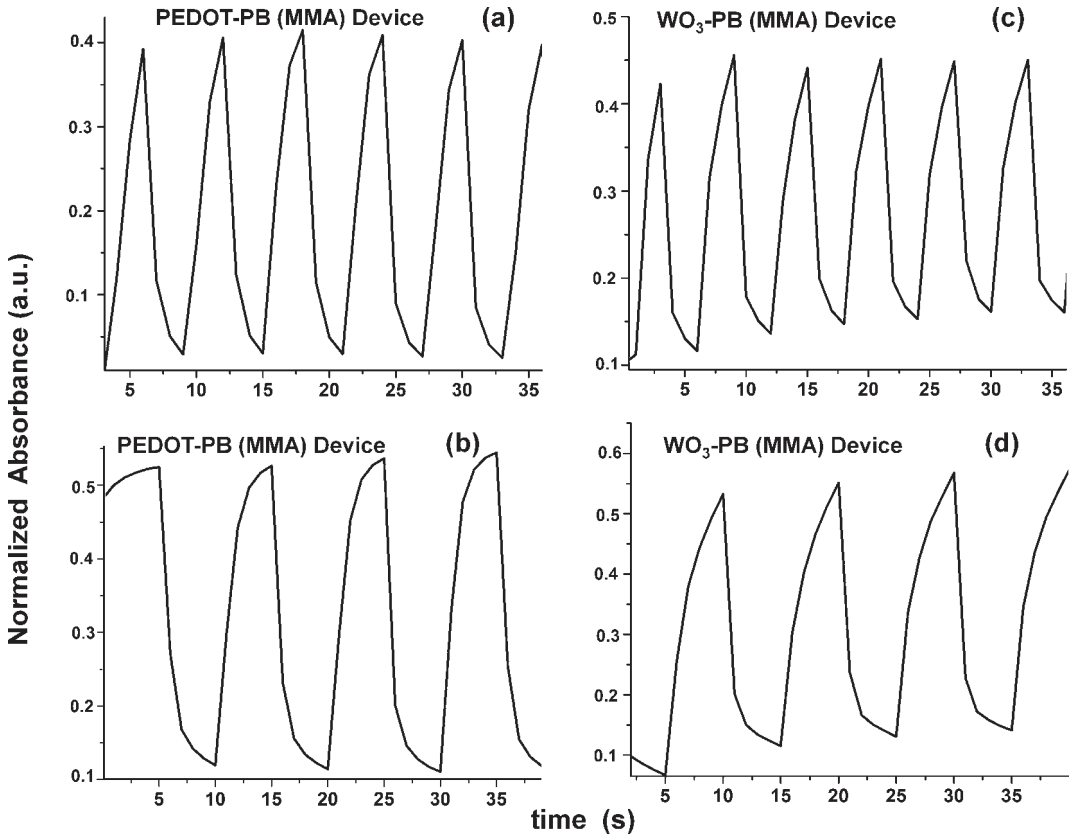

Fig. 7 Color-bleach kinetics of a PEDOT–PB (MMA) device recorded at a λ_{max} of 585 nm with a step time of (a) 3 s and (b) 5 s and of a WO_3–PB (MMA) device at a λ_{max} of 685 nm with a step time of (c) 3 s and (d) 5 s.

to the neutral state; the ease of electron injection into the matrix of a not yet insulating film promotes faster color kinetics. Color and bleach times of 13 s and 5 s were achieved for a WO_3 nanorod film, in a $LiClO_4$–PC solution under applied potentials of ± 3 V,[34] and for a PANI–WO_3 device a coloring time of $\sim$17 s was registered.[9] The PMMA based devices showed slower kinetics and a smaller magnitude of optical density change (Fig. S5, ESI†) for the same values of applied potential as used for the MMA based devices. Moderately fast switching kinetics shown by MMA based devices renders them suitable for smart window applications. To further confirm that absorbance in the visible region indeed changes rapidly in PEDOT film, the dynamic change in absorbance was measured during redox switching. The films were subjected to an oxidation potential of +1.0 V for 3 s, and the dynamic absorbance, wherein the instrument scans the 300–800 nm wavelength range within 1 ms, was measured. In a similar manner, dynamic spectral responses of the same film were recorded under a reduction potential of −1.0 V for durations of 10, 15, 20, 25 and 30 s (Fig. 8). The film acquires a saturated blue color within 25 s, as the dynamic response measured for a 30 s duration re-traces the curve obtained in the 25 s cycle. From the curves it is obvious that the film acquires $\sim$69% of the total absorption change that it is capable of attaining, within 5 s. This is a clear indicator of the fact that film shows fast kinetics. Bleaching is also fast, as the peak due to π–π* absorption vanishes in a span of 3 s.

3.6. Electrochemical impedance spectroscopy

Nyquist plots of WO_3–PB (MMA), WO_3–PB (PMMA), PEDOT–PB (MMA) and PEDOT–PB (PMMA) devices are shown in Fig. 9a and b and Bode plots are shown in the

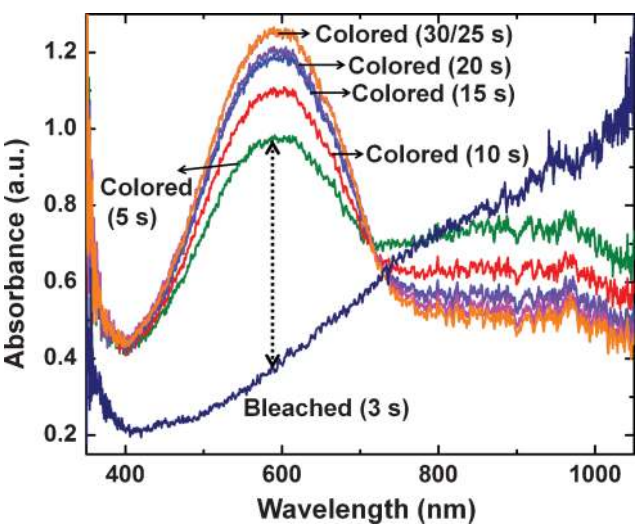

Fig. 8 Dynamic absorbance spectrum of a PEDOT film, recorded in a liquid electrolyte, wherein the wavelength range $\sim$400 to 800 nm is swept within 1 ms, under dc potentials of +1.0 V (for bleaching) and −1.0 V (for coloration).

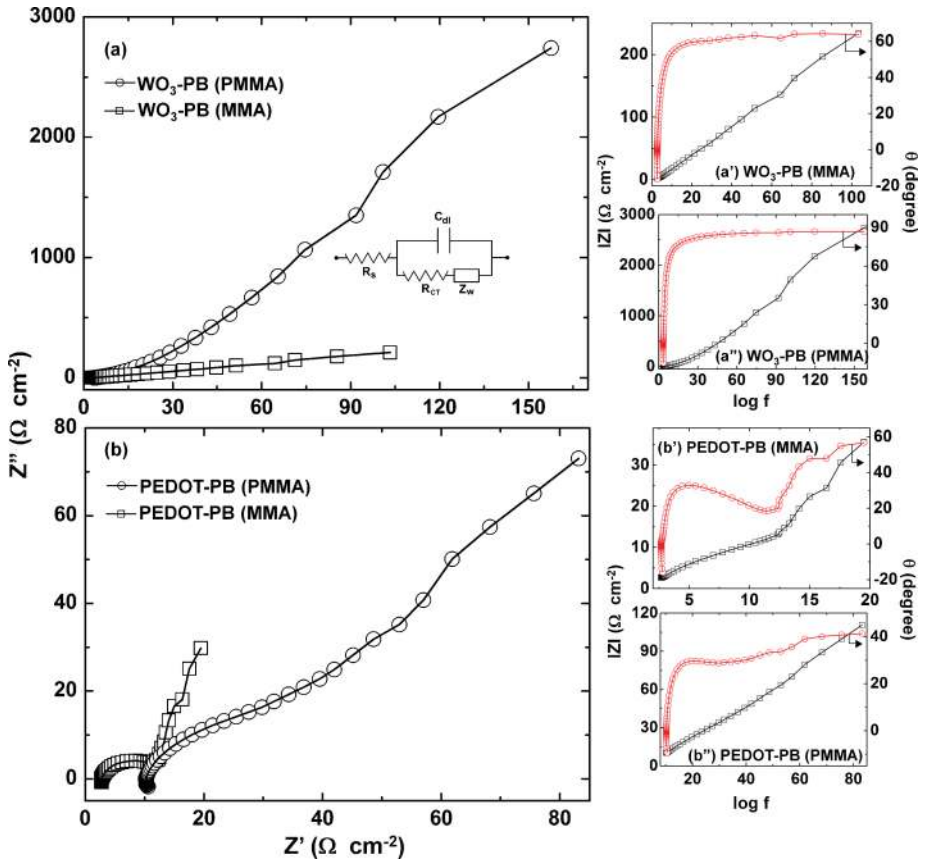

Fig. 9 Nyquist plots of (a) WO_3–PB(MMA) (□) and WO_3–PB(PMMA) (○) devices and (b) PEDOT–PB (MMA) (□) and PEDOT–PB (PMMA) (○) devices recorded under an ac amplitude of 10 mV; (a′, a″, b′ and b″) are the corresponding Bode plots (□) $|Z|$ *versus* log (frequency) and (○) θ *versus* log (frequency). The symbols represent the experimental data and the solid lines (—) are obtained by fitting the experimental data in the model shown in (a).

corresponding panels. The equivalent circuit displayed in Fig. 9a was found to give excellent fits for all Z'' *versus* Z' curves and the fitted/calculated parameters are summarized in Table S2 (ESI†). The PEDOT–PB (MMA) device shows an arc in the high frequency region, whereas only a slight curvature is observed for the PEDOT–PB (PMMA) device. For the WO_3–PB devices, a nearly straight line behavior is observed, which is characteristic of fast charge transfer at the SnO_2:F–WO_3, WO_3–electrolyte interfaces, and also of rapid ion transport through the bulk of the WO_3 film. As can be seen from the Bode plots, the magnitude of impedance ($|Z|$) is larger for the PMMA based devices in comparison to the MMA based devices. The ionic conductivities of the two electrolytes were determined from the impedance plots, and for the MMA based gel it is 1.6×10^{-4} S cm^{-1}. The PMMA based gel shows an ionic conductivity of 4.2×10^{-5} S cm^{-1}. In the past, a poly(ethyl methacrylate)–$LiClO_4$–PC based electrolyte showed a room temperature ionic conductivity of 6.9×10^{-4} S cm^{-1} [14] and a dried polyelectrolyte film of poly(ethylene imine)–poly(acrylic acid)–$LiCF_3SO_3$, prepared by a layer-by-layer assembly method, was characterized by an ionic conductivity greater than 10^{-5} S cm^{-1} at ambient temperature.[16] The charge transfer resistances (R_{CT}) for the MMA based devices are smaller in magnitude compared to the PMMA based devices (Table S2, ESI†). It is apparent that the MMA based electrolyte forms a more intimate contact with the electrode (PEDOT or WO_3) surface as it is introduced into the device in a liquid state, in contrast to the PMMA based electrolyte, which, is incorporated in a semi-solid state and therefore does not attach to the electrode as effectively as the MMA electrolyte does. This inference is also supported by the fact that both exchange current density and diffusional pseudocapacitance (the measure of charging in the bulk of the film in the low frequency region) have larger values for the MMA based devices in contrast to the PMMA based devices (Table S2, ESI†).

4. Conclusions

Two methods were used for synthesizing and applying polymer electrolytes to electrochromic devices of WO_3–PB and PEDOT–PB. In the first approach, a homogeneous transparent gel formed by immobilization of PMMA in an ionic liquid was applied to the devices, whereas in the second method direct *in situ* thermal polymerization of the monomer in the devices was performed after injecting the MMA-ionic liquid solution into the devices. The *in situ* polymerized gel, by virtue of being introduced into the device in a liquid state, allows the formation of better interfacial contacts, which reduces the charge transfer resistance and thus enables faster intercalation–deintercalation reactions at the electrochromic electrode. It also allows a greater number of electrolyte ions to access the redox active sites in the electrochromic films, which results in high contrast, thus resulting in a

coloring efficiency of 119 $cm^2\ C^{-1}$ (λ_{max} = 550 nm) for the WO_3–PB (MMA) based device as compared to a CE of 54 $cm^2\ C^{-1}$ at the same wavelength for the WO_3–PB (PMMA) based device. The role of film microstructure was found to affect ion insertion–extraction kinetics, and therefore the open channels provided by the four/six/three coordinated voids created by the hexagonal crystal structure of the WO_3 film impacted bleaching kinetics favorably. Devices prepared by direct incorporation of the gel electrolyte, do not have either of the above mentioned two advantages and therefore the electrochromic performance is adversely affected. Large area devices were successfully fabricated using the *in situ* polymerized gel and their ability to color uniformly without any pinholes or color gradients indicates the promise this method holds for further upscaling and application to commercial electrochromic devices.

Acknowledgements

Financial support from Department of Science & Technology (DST/TSG/PT/2007/69) is gratefully acknowledged. One of the authors, Rambabu Sydam acknowledges DST and University Grants Commission for junior research fellowship.

References

1 D. T. Gillaspie, R. C. Tenent and A. C. Dillon, *J. Mater. Chem.*, 2010, **20**, 9585.
2 S. V. Vasilyeva, P. M. Beaujuge, S. Wang, J. E. Babiarz, V. W. Ballarotto and J. R. Reynolds, *ACS Appl. Mater. Interfaces*, 2011, **3**, 1022.
3 G. A. Niklasson and C. G. Granqvist, *J. Mater. Chem.*, 2007, **17**, 127.
4 C. G. Granqvist, *Handbook of Inorganic Electrochromic Materials*, Elsevier, Amsterdam, 1995.
5 P. M. S. Monk, R. J. Mortimer and D. R. Rosseinsky, *Electrochromism and Electrochromic Devices*, Cambridge University Press, United Kingdom, 2007.
6 P.-H. Aubert, A. A. Argun, A. Cirpan, D. B. Tanner and J. R. Reynolds, *Chem. Mater.*, 2004, **16**, 2386.
7 C. S. Blackman and I. P. Parkin, *Chem. Mater.*, 2005, **17**, 1583.
8 S. Kirchmeyer and K. Reuter, *J. Mater. Chem.*, 2005, **15**, 2077.
9 L. Zhang, S. Xiong, J. Ma and X. Lu, *Sol. Energy Mater. Sol. Cells*, 2009, **93**, 625.
10 A. A. Argun, A. Cirpan and J. R. Reynolds, *Adv. Mater.*, 2003, **15**, 1338.
11 A. Kumar, D. M. Welsh, M. C. Morvant, F. Piroux, K. A. Abboud and J. R. Reynolds, *Chem. Mater.*, 1998, **10**, 896.
12 R. J. Mortimer and J. R. Reynolds, *J. Mater. Chem.*, 2005, **15**, 2226.
13 C. A. Nguyen, S. Xiong, J. Ma, X. Lu and P. S. Lee, *J. Phys. Chem. B*, 2009, **113**, 8006.
14 J. Reiter, O. Krejza and M. Sedlarkova, *Sol. Energy Mater. Sol. Cells*, 2009, **93**, 249.
15 E. D. C. Rios, A. V. Rosario, A. F. Nogueira and L. Micaroni, *Sol. Energy Mater. Sol. Cells*, 2010, **94**, 1338.
16 C. A. Nguyen, A. A. Argun, P. T. Hammond, X. Lu and P. S. Lee, *Chem. Mater.*, 2011, **23**, 2142.
17 J. Zhang, J. P. Tu, X. H. Xia, Y. Qiao and Y. Lu, *Sol. Energy Mater. Sol. Cells*, 2009, **93**, 1840.
18 C.-Y. Kim, S.-G. Cho and T.-Y. Lim, *Sol. Energy Mater. Sol. Cells*, 2009, **93**, 2056.
19 F. Tran-Van, L. Beouch, F. Vidal, P. Yammine, D. Teyssie and C. Chevrot, *Electrochim. Acta*, 2008, **53**, 4336.
20 L. Su, J. Fang, Z. Xiao and Z. Lu, *Thin Solid Films*, 1997, **306**, 133.
21 S. I. Cho and S. B. Lee, *Acc. Chem. Res.*, 2008, **41**, 699.
22 D. DeLongchamp and P. T. Hammond, *Adv. Mater.*, 2001, **13**, 1455.
23 S. Duluard, A. C. -Cochet, I. Saadeddin, A. Labouret, G. Campet, G. Schottner, U. Posset and M.-H. Delville, *New J. Chem.*, 2011, **35**, 2314.
24 M. Deepa, A. Awadhia and S. Bhandari, *Phys. Chem. Chem. Phys.*, 2009, **11**, 5674.
25 M. Deepa, A. Awadhia, S. Bhandari and S. L. Agrawal, *Electrochim. Acta*, 2008, **53**, 7266.
26 M. Dobbelin, I. Azcune, M. Bedu, A. R. de Luzuriaga, A. Genua, V. Jovanovski, G. Cabanero and I. Odriozola, *Chem. Mater.*, 2012, **24**, 1583.
27 T. Sato, G. Masuda and K. Takagi, *Electrochim. Acta*, 2004, **49**, 3603.
28 R. M. Osuna, V. Hernandez, J. T. L. Navarrete, E.I. Kauppinen and V. Ruiz, *J. Phys. Chem. Lett.*, 2010, **1**, 11367.
29 S. Balaji, Y. Djaoued, A.-S. Albert, R. Z. Ferguson and R. Bruning, *Chem. Mater.*, 2009, **21**, 1381.
30 W. B. Hu, Y. Q. Zhu, W. K. Hsu, B. H. Chang, M. Terrones, N. Grobert, H. Terrones, J. P. Hare, H. W. Kroto and D. R. M. Walton, *Appl. Phys. A: Mater. Sci. Process.*, 2000, **70**, 231.
31 M. Deepa, A. K. Srivastava, S. Lauterbach, G. S. M. Shivaprasad and K. N. Sood, *Acta Mater.*, 2007, **50**, 6095.
32 S. Bhandari, M. Deepa, S. Pahal, A. G. Joshi, A. K. Srivastava and R. Kant, *ChemSusChem*, 2010, **3**, 97.
33 K.-C. Chen, C.-Y. Hsu, C.-W. Hu and K.-C. Ho, *Sol. Energy Mater. Sol. Cells*, 2011, **95**, 2238.
34 J. Wang, E. Khoo, P. S. Lee and J. Ma, *J. Phys. Chem. C*, 2008, **112**, 14306.